Microporous and Mesoporous Materials 345 (2022) 112246

Contents lists available at ScienceDirect

Microporous and Mesoporous Materials

journal homepage: www.elsevier.com/locate/micromeso

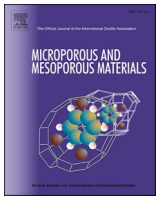

Enhanced mechanical stability and scratch resistance of mesoporous aluminosilicate thin films

Barry Reid [a], Ishaa Mane [a], Faizah Ahmed [a], Maximiliano Jara Fornerod [a], Máté Füredi [a], Benjamin Schmidt-Hansberg [b], Alberto Alvarez-Fernandez [a,*], Stefan Guldin [a,*]

[a] Department of Chemical Engineering, University College London, Torrington Place, London, WC1E 7JE, United Kingdom
[b] Chemical & Process Engineering, Coating & Film Processing, BASF SE, Carl-Bosch-Strasse 38, Ludwigshafen Am Rhein, 67056, Germany

ARTICLE INFO

Keywords:
Mesoporous
Thin-film
Mechanical properties
Co-assembly
Scratching
Block copolymers

ABSTRACT

Mesoporous coatings are widely used in industries such as optics, display technologies, photovoltaics, and bioengineering, due to their attractive properties such as high surface area to volume ratio and excellent mass and electron transport characteristics. While structural parameters and material composition can be routinely tailored to the respective applications, improvements in their mechanical properties and robustness, essential for their long-term performance, remain a challenge. Herein, we provide a comprehensive study on the relationship between the degree of porosity, type of material processing and resulting mechanical properties for the use case of mesoporous aluminosilicate thin films that were co-assembled via a sacrificial block copolymer structure-directing agent. Several routes, including the introduction of chelating agents on the precursor solution, a two-step calcination process, and a variation over the aluminium content were explored with the objective of improving the scratch resistance and mechanical properties of the final mesoporous thin film. Pencil hardness tests were combined with atomic force microscopy analysis to investigate the macroscopic scratch resistance, i.e. plastic deformation. Ellipsometric porosimetry served to determine the elastic deformation of the nanoscopic architecture via measurement of the Young's modulus. Our comparative investigation highlights the promising role of organic chelating agents in the sol-gel formulation to slow down the hydrolysis of the aluminium precursor, which facilitated improvements in the mechanical performance close to industrial standard.

1. Introduction

The use of mesoporous thin films as coatings has become increasingly important in applications such as storage devices [1], integrated circuits, semiconductor devices, anti-reflective coatings [2–4], photovoltaics [5,6], biosensors [7,8], and separation membranes [9]. Many of these applications require the introduction of mesoporous coatings with high porosity and pore size to wall thickness ratio, in order to improve their optical as well as charge and mass transport properties, respectively.

Different approaches have been developed to prepare such materials, including the random packing of nanoparticles [10,11] as well as surfactant templating [12–14], replication [15,16], or colloidal and block copolymer co-assembly of inorganic material often derived by sol-gel chemistry [17–19]. Typically, the use of a sacrificial organic porogen or structure-directing agent provides access to control over the porosity of the resulting mesoporous inorganic coating. However, the induced porosity results in unfavourable mechanical properties of the coatings, reducing their structural integrity and scratch resistance and compromising their long-term performance [20].

Numerous strategies have been reported to improve the mechanical characteristics of mesoporous films by either modifying the formulation of the precursor solution or via post-coating film treatment [20]. Pre-coating modifications include the addition of reflux and sol additives such as tetrapropylammonium hydroxide to the inorganic solution, promoting the condensation reaction between silanols groups, and improving the mechanical strength of the final mesoporous films while keeping high porosity values [21]. Alternatively, the addition of harder metallic elements such as organofunctional metal alkoxides or metallic nanoparticles has shown the possibility of modifying the final mesoporous materials, achieving values as high as 5H pencil hardness [22,23]. Others have explored the addition of cross-linker molecules to improve the extent of inorganic condensation [24]. To this end, Wu and co-workers reported improved scratch resistance of mesoporous silica

* Corresponding author.
E-mail addresses: alberto.fernandez@ucl.ac.uk (A. Alvarez-Fernandez), s.guldin@ucl.ac.uk (S. Guldin).

https://doi.org/10.1016/j.micromeso.2022.112246
Received 20 July 2022; Received in revised form 15 September 2022; Accepted 21 September 2022
Available online 26 September 2022

films (from 2 B to 5H) by adjusting the quantity of ethylenediamine added to the precursor solution [24]. The addition of this cross-linker molecule was found to promote the opening of the epoxy ring of (3-Glycidyloxypropyl)trimethoxysilane (GLYMO) monomers and increase the crosslinking density within the coating [25].

On the other hand, post-deposition processing methods have been generally focused on improving the degree of condensation within the inorganic network to create denser inorganic structures. This has been achieved using high-temperature calcination [26–28], UV curing [29], and post-synthetic vapour treatments with water [30], ammonia [31,32], and silane vapours [33–35]. More complex structures and coatings were developed to improve both the mechanical and antireflective characteristics of porous thin films [36,37]. To this end, ultra-thin TiO_2 capping layers were found to improve scratch resistance and self-cleaning in SiO_2-based anti-reflective coatings [38].

Despite this extensive research, improvements in the mechanical stability of highly porous mesoporous thin films remain limited. One attractive approach to overpass this limitation relies on the incorporation of chelating agents into the sol-gel recipe. Organic moieties such as acetylacetone (AcAc) or ethyl acetoacetate (EtOAcAc) have shown their efficiency in slowing down the hydrolysis of inorganic precursors [39–41]. Thus, their addition for example to aluminium tri-*sec*-butoxide allowed handling of the solutions even under ambient conditions. The addition of chelating agents provides access to stable and precipitation-free sol-gel precursor solutions [42,43]. The slower condensation kinetics allow the formation of denser inorganic networks, by reducing the intrinsic microporosity of the inorganic material produced during the sol-gel condensation [44]. This can be expected to have an impact on the mechanical properties of the films. However, such study remains unexplored.

Another challenge involves the search for suitable techniques for the assessment of the mechanical properties of mesoporous thin films due to the small total surface area and pore volume of the active film and background signal from the underlying substrate. Scratch and abrasion resistance are commonly assessed by qualitative test methods, which are regulated by the International Organisation for Standardisation (ISO). These tests include pencil hardness [45], wiping [46], washing [47], adhesive tape [48], and rotating abraders [49]. The aforementioned approaches rely on qualitative visual inspection via optical or scanning electron microscopy. Recently, image analysis techniques have been employed to improve the accuracy of such inspection and provide a route toward quantification of film removal during abrasion tests [49]. For more quantitative scratch resistance analysis, nano-scratch instrumentation employs nano-indenters of specific geometry to apply a measurable load to a film. The visual identification of film delamination and buckling can then be related to a specific load applied [50]. However, this increases the cost and complexity of scratch resistance assessment.

Young's modulus (E), also known as elastic modulus, is defined as the ability of a material to withstand changes in length when under uniaxial tension. This comprises an important characteristic for materials that require multiple processing and packaging steps [16,51]. One example is found in low-k materials, which are crucial for improving the integrated circuit performance of semiconductor devices [52,53]. During manufacturing processes, materials with low E are susceptible to thermal and mechanical stresses, which may lead to delamination or cohesive failure [53,54]. Coatings with E below 10 GPa pose some challenges for industrial processing, yet E values of $\approx$ 4 GPa were found to still withstand common mechanical planarization processes [55].

The aforementioned techniques are prevalent when reporting the film modulus and hardness. However, there are concerns about overestimating the film hardness due to the contribution of the substrate, especially in films of thickness in the range of hundreds of nanometers [56–59]. To this end, surface acoustic wave spectroscopy (SAWS) [60,61], Brillouin light scattering (BLS) [62], and X-ray reflectivity [28] were developed as alternatives to NI methods. While these techniques have demonstrated effectiveness for non-destructive E measurement, disadvantages include requirements for X-rays, specialised substrates [63], and high-resolution interferometry instrumentation [64].

In recent years, ellipsometric porosimetry (EP) has been identified as a non-destructive technique for Young's modulus calculation [65]. This approach is based on monitoring the film thickness contraction during capillary condensation and subsequent thickness relaxation. EP removes the influence of the substrate from modulus calculations, while also allowing for simultaneous non-destructive measurement of porosity and pore size distribution. EP calculation of E demonstrated agreement with SAWS and BLS but with the advantage of concurrent porosity and pore size measurement, making it a powerful technique for the comprehensive analysis of porous thin films [66].

In this work, the scratch resistance and mechanical properties of mesoporous aluminosilicate thin films, fabricated following previously established BCP co-assembly strategy [67–69], are investigated, with a particular focus on the effect of structural characteristics, processing conditions, and addition of chelating agents to the sol-gel precursor solution. These results are benchmarked against the mechanical properties of coatings derived from commercially available colloidal silica materials. While pencil hardness tests provide an overview of the macroscopic scratch resistance, i.e. plastic deformation, EP measurements enable quantitative determination of the nanoscopic Young's modulus, i.e. elastic deformation. Ultimately, this study aims to provide an overview of the relationship between structural characteristics, material processing and the resulting mechanical properties, providing guidelines for future approaches under design constraints.

2. Experimental

2.1. Materials

$PIB_{3.9k}$-b-$PEO_{3.6k}$ block copolymer (polydispersity 1.26, Mn 4.85 kg/mol^{-1}) was provided by BASF [70]. Toluene (99.9%), 1-butanol (99.4%), aluminium tri-*sec*-butoxide (97%), (3-glycidyloxypropyl)--trimethoxysilane (GLYMO) (≥98%), potassium chloride (KCl) (≥99.9%) and acetylacetone (for synthesis) were purchased from Sigma-Aldrich. All chemicals were used without further purification.

2.2. Preparation of the mesoporous aluminosilicate thin films

Aluminosilicate sol was prepared as described in previous studies [71–74]. In short, 2.8 g of (3-glycidyloxypropyl)trimethoxysilane (GLYMO, ≥ 98%, Sigma Aldrich) was mixed with 0.32 g of aluminium tri-*sec*-butoxide (ALTSB, 97%, Sigma Aldrich) (molar ratio 9:1) and 20 mg of KCl (≥99.9%, Sigma Aldrich). The solution was then stirred vigorously in an ice batch for 15 min. In a first hydrolysis phase, 0.135 mL of 10 mM hydrochloric acid (HCl, 37%, Merck) was slowly added dropwise. The solution was stirred for another 15 min before it was removed from the ice bath and stirred for another 15 min at room temperature. In a second hydrolysis phase, 0.85 mL of 10 mM HCl was added dropwise, and the mixture was stirred for another 20 min. The as-made sol was then diluted with the azeotrope solvent mixture to a concentration of 1000 mg/mL and stored at 5 °C for further use, with a shelf life of at least one month.

Inorganic sol was incorporated into the block copolymer stock solution (40 mg/ml in an azeotrope solution of toluene/1-butanol (72.84/27.16 wt%)) in volumes described in Table 1 to produce the so-called hybrid solution and left mixing in a shaker for 30 min before use. 80 μl of the hybrid solution was subsequently spin-coated onto silicon substrates (2000 rpm, 20 s, Laurell WS 650 MZ). In the case of the chelating agent solution, 1.4 mmol of AcAc was added to the sol solution. Thin films were subsequently calcined. Films processed via a so-called "one-step calcination" were calcined in air at 450 °C (30 min, 5 °C/min^{-1}). Films made by "two-step calcination" were first annealed in argon at 450 °C (30 min, 5 °C/min^{-1}) in a tubular furnace, and

Table 1
Block copolymer and aluminosilicate volumes used to generate a hybrid solution with BCP content of 20, 30 and 40%.

Sample	Block copolymer	Block copolymer content [% mass]	BCP stock solution [μl]	Aluminosilicate stock solution [μl]
BCP_{20}	PIB-*b*-PEO	20	469	120
BCP_{30}	PIB-*b*-PEO	30	469	70
BCP_{40}	PIB-*b*-PEO	40	469	45

subsequently air calcined at 450 °C (30 min, 5 °C/min^{-1}). All films were cooled down inside the furnace.

2.3. Preparation reference samples

Ludox TMA colloidal silica nanoparticles (34 wt % suspension in H2O) were purchased from Sigma Aldrich and diluted to one quarter of the original concentration in water before spin coating at 5000 rpm. Thin films prepared from Ludox solutions (SiLudox) were tested either after air drying at ambient temperature or additional high-temperature treatment at 450 °C for 30 min.

2.4. Assessment of scratch resistance using pencil hardness test

To assess the scratch resistance of films, pencil hardness tests were performed using a manual Elcometer 501 pencil hardness tester in accordance with the standard American Society for Testing and Materials (ASTM) D3363 method [75]. Varying hardness values (from 5 B to 5H) graphite pencils were maintained at a constant angle of 45° while exerting a downward force of 7.5 N when applied over the coatings (see Fig. S1). In this work, the gouge hardness (defined as the appearance of several scratches and/or removal of a significant portion of the film) was considered the main method for assessing the scratch resistance. Early-onset of single scratches were observed at times, which was attributed to the manual nature of the pencil lead preparation process [75]. All pencil scratch images were acquired and visually assessed using a Zeiss Axioscope A1 with 5× magnification.

2.5. Porosity, pore size, and Young's modulus calculation using ellipsometric porosimetry

Ellipsometric porosimetry (EP) measurements were carried out on a Semilab SE-2000 variable angle spectroscopic ellipsometer in the spectral range. During ellipsometric porosimetry measurements with water, spectra were obtained at minimum of 30 individual p/p_0 steps (in the range between 0.5% and 100%) to construct the adsorption and desorption isotherms from the fitted refractive index values. For the measurements using methanol as adsorptive, spectra were obtained similarly at minimum of 30 individual p/p_0 steps inside a vacuum chamber with a proportional valve connected to the adsorptive vessel for precise pressure control [76]. Pore size distributions were calculated from the former water adsorbed/desorbed isotherms based on the modified Kelvin-equation.

Young's modulus (E) measurements were performed to assess the stiffness of the material. E values provide a quantitative assessment of the mechanical characteristics to complement the qualitative observations from pencil scratch tests. Ellipsometric porosimetry (EP) measurements were carried out on a Semilab SE-2000 variable angle spectroscopic ellipsometer in the spectral range of 300–900 nm. EP desorption curves were fitted using Equations 1 and 2.

$$\pi_c = ln\ \frac{P}{P_0}\frac{RT}{V_L} \tag{1}$$

where π_c is defined as the microscopic capillary pressure, P/P_0 as the relative pressure, and V_L the water molar volume. The film thickness evolution (d, d_0) was then related to E as follows:

$$d = d_0 - k\ ln\frac{P}{P_0} \tag{2}$$

Where $k = d_0RT/V_LE$. A linear fit of the film shrinkage during desorption enables the calculation of E using Equation (2). The desorption isotherm is used for the linear fit since incremental and non-uniform pore filling influences film thickness measurements during adsorption, while desorption typically exhibits more uniform pore emptying [77]. All data analysis was performed using the Semilabs SEA software (v1.6.2).

2.6. Grazing-incidence small-angle x-ray scattering (GISAXS

GISAXS experiments were conducted on a SAXSLab Ganesha (8 keV). The incidence angle was set at 0.2°. 2D scattering patterns were collected with a PILATUS 300 K solid-state photon-counting detector at a sample-to-detector distance of 950 mm. GISAXS data analysis was accomplished with the FitGISAXS software [78].

2.7. Atomic force microscopy (AFM)

AFM images were obtained on a Bruker Dimension Icon atomic force microscope with a Bruker ScanAsyst Air probe (nominal tip radius 2 nm) in PeakForce tapping (PFT) mode.

2.8. Scanning electron microscopy (SEM)

SEM images were captured in an Xbeam 540 FIB/SEM (ZEISS) directly on the film surface without applying any conductive coating by using a low acceleration voltage (0.5–2 kV) and short working distance (~1 mm).

3. Results and discussion

As previously introduced, the use of block copolymers (BCPs) as sacrificial structure-directing agent via micelle co-assembly provides a large degree of freedom for the resulting inorganic mesoporous thin film architectures with regards to porosity, pore size and pore arrangement [69]. This makes BCP co-assembly a particularly suitable fabrication approach to study the influence of a variety of structural and experimental parameters on the mechanical properties of mesoporous thin films. Specifically, the effect of three independent experimental factors on the mechanical properties (scratch resistance and Young's modulus) was studied during this work: (A) the total porosity, (B) the addition of chelating agents to the precursor solution and (C) the introduction of a two-step Ar/O_2 calcination process (see Fig. 1). Each of these processes is presented in the following sections.

3.1. Effect of porosity

One of the most important advantages of the use of block copolymers (BCP) as sacrificial structure-directing agents via micelle co-assembly is the possibility of fine-tuning the total porosity of the inorganic sample by controlling the organic to inorganic (O:I) ratio in the formulation. Hybrid solutions with different O:I ratios were deposited onto silicon substrates by spin-coating (samples AlSi-20; AlSi-30 and AlSi-40 respectively). The grazing-incidence X-ray Scattering (GISAXS) pattern of the hybrid film exhibits a degree of ordering and peaks corresponding to a hexagonally packed structure (Fig. S2). EP adsorption isotherms after the calcination and subsequent polymer removal confirm the formation of a porous structure. The hysteresis loops present in the adsorption-desorption isotherms verify the formation of ellipsoidal mesoscale pores with narrow interconnections. Increasing porosity values of 35 ± 0.8 (AlSi-20); 49 ± 0.6 (AlSi-30) and 60 ± 0.5% (AlSi-40)

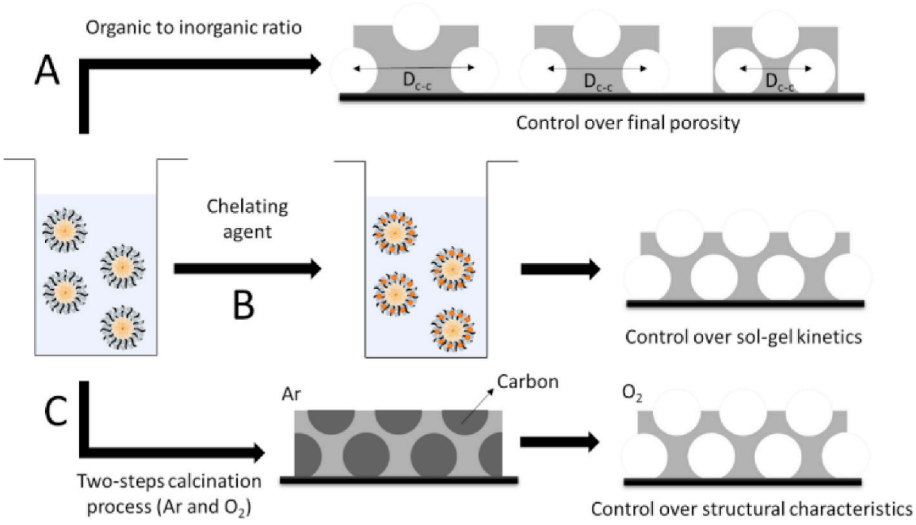

Fig. 1. Schematic of the different approaches pursued during this work for improving the mechanical properties of aluminosilicate mesoporous films: A) variation of porosity, B) addition of chelating agent to the sol-gel precursor solution and C) modification of the processing conditions with two-step calcination (initially under inert atmosphere).

were measured, which were scaled according to the O:I ratios in the starting solution (20, 30 and 40% organic content respectively), see Fig. 2A–C.

EP provides a reliable method for the determination of total porosity in mesoporous thin films [73,79]. Contrary to more commonly used techniques to study surface morphology (like scanning electron or atomic force microscopy), EP probes the accessible porosity across the entire film thickness and for a representative sample volume [71,72,80]. Moreover, EP provides also information about pore size distribution and the Youngs modulus [77,81]. As shown in the Supporting Information (Fig. S3), some changes were also observed with the modification over the O:I ratio: 7.2 ± 0.1 nm (AlSi-20); 8.2 ± 0.3 nm (AlSi-30) and 10.0 ± 0.1 nm (AlSi-40), which is in agreement with previous studies [69], Young's modulus (*E*) values were obtained from the fitting of the EP measurements (Fig. 2D). A clear decrease in Young's modulus was found with increasing porosity from the EP measurements (Fig. 2E) or in return, the lower the porosity, the stiffer the films. Samples with high inorganic content, and therefore low porosity (AlSi-20) displayed an *E* of 3.4 ± 0.3 GPa. This value was significantly reduced to 1.3 ± 0.2 GPa for samples with higher porosity (AlSi-30) and reached its minimum value for the highest porous films (AlSi-40) with 0.6 ± 0.1 GPa.

Scratch tests were performed on samples from the three different O:I

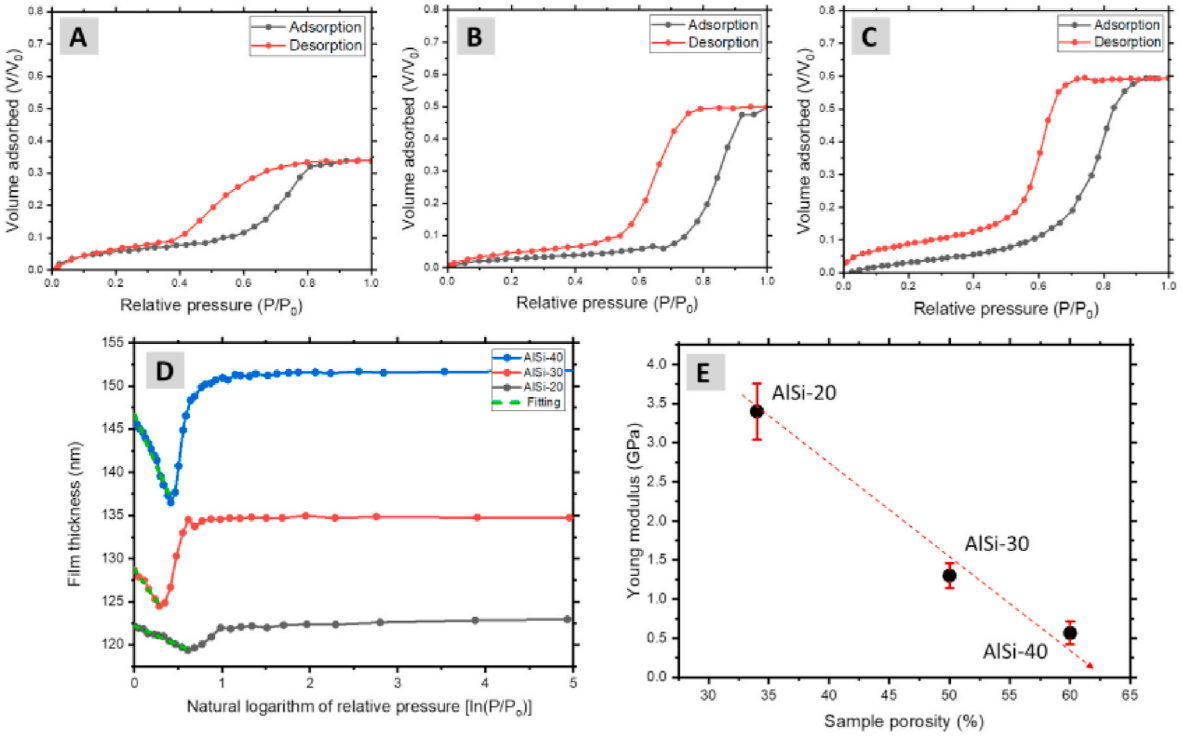

Fig. 2. EP absorption-desorption isotherms (A–C) and corresponding thickness isotherms plotted in the log p/p_0 scale (D) for samples with varying porosity, linear fit shown in green. AlSi-20 (A); AlSi-30 (B) and AlSi-40 (C). Evolution of Young's modulus with the change in the porosity of the samples (E). (For interpretation of the references to colour in this figure legend, the reader is referred to the Web version of this article.)

ratios. Fig. 3 displays representative optical microscopy images of the scratch tests, in which the pencil hardness for the first damage of the respective coatings was detected (see Fig. S4 for more details). From the images, a clear trend in deterioration of scratch resistance with increasing porosity was detected. The gouge hardness was reduced from 3H for a 35% porosity sample (AlSi-20, Fig. 3A), to 2H for 49% porosity (AlSi-30, Fig. 3B), and 6B for 60% porosity samples (AlSi-40, Fig. 3C). These trends correlate closely with results previously reported by other authors [30,82,83]. A comparison of results in this section to benchmark values (Fig. S5) shows that the mesoporous aluminosilicate samples obtained by BCP co-assembly perform significantly better than coatings with similar porosity obtained by the random packing of silica nanoparticles (Ludox) and compare favourably with published scratch resistance data as summarized in Table S1 and **S2.** Thus, while the inclusion of porosity generally has a negative impact on the mechanical properties of thin films, establishing suitable processing conditions that control the structural characteristics of the porous architecture can help to minimize this effect.

In order to confirm the impact of the nanoscopic structural control on the mechanical properties of the created thin films, AFM measurements were performed on an AlSi-20 sample after scratching with a 2H pencil (Fig. 4). Importantly, the presence of pores underneath the pencil scratch was still depicted, providing evidence that the pencil scratch did not cause major damage to the network of pores underneath. Fig. S6 shows a height profile extracted from the 2H pencil scratched area. The average pencil scratch depth was 14 nm, which equated to ≈12% of the film thickness, indicating that the 2H pencil only removed a small amount of material from the film surface.

3.2. Control over sol-gel kinetics

As previously introduced, due to the rapid nature of the hydrolysis and condensation reactions of metallic alkoxide precursors, chelating agents have been widely employed to slow down hydrolysis reaction rates and prevent precipitation and/or formation of large agglomerates [39–41]. Aluminium tri *sec*-butoxide contains three reactive sites (Fig. 5A) that are susceptible to rapid hydrolysis and gelation. Diketones and -keto esters such as acetylacetone (AcAc) and ethyl acetoacetone (EtOAcAc) have been introduced to control the kinetics of the hydrolysis [40,84]. These chelating agents were reported to slow down the condensation process by blocking reaction sites (shown on the right-hand side of Fig. 5A), while still allowing the formation of tetrahedrally coordinated aluminium and Al–*O*–Si bonds during the sol-gel process [84]. In the following, the effect of AcAc addition to the initial sol-gel recipe on the mechanical properties of the resulting mesoporous thin films is presented. Hybrid solutions with different O:I ratios and chelating agent content were deposited onto silicon substrates by spin-coating.

Grazing-incidence X-ray scattering (GISAXS) patterns of the hybrid films provide evidence that the addition of the chelating agent to the inorganic precursor solution did not affect the degree of order (Fig. 5B), thus maintaining the hexagonal packing observed in the previous section (Fig. S2). Adsorption isotherms of the inorganic mesoporous coatings obtained after calcination of the hybrid films show an increasing porosity, related to the O:I content in the starting solution (Fig. 6A–C). While for a 20% organic content sample a total porosity of 38 ± 0.7% (AcAc-20) was obtained, values increased to 48 ± 0.6 and 59 ± 0.8% for a 30% (AcAc-30) and 40% (AcAc-40) organic content, respectively. Thus, the addition of the chelating agent to the inorganic precursor solution did not have an effect on the total mesoscale porosity of the created inorganic films, allowing a direct comparison with previous results.

Similarly to the previous section, mechanical properties were evaluated by EP and pencil hardness tests, respectively. In the case of the former, EP fittings show an increase in the elasticity of the aluminosilicate film with increased porosity, a similar trend to the previous results with standard aluminosilicate precursors. However, a clear improvement in absolute values was observed with the addition of the chelating agent. The presence of the AcAc on the hybrid films led to an increase in E from 3.4 ± 0.5 (AlSi-20) to 4.3 ± 0.7 GPa (AcAc-20) in the case of the 20% organic content film, after calcination. Corresponding results of 1.6 ± 0.2 and 0.9 ± 0.1 GPa were observed for 30% (AcAc-30) and 40% (AcAc-40) organic content, improving previously obtained values for the reference samples without chelating agent of 1.3 ± 0.1 (AlSi-30) and 0.6 ± 0.1 GPa (AlSi-40) (Fig. 6D and E). It is important to highlight the 4.3 ± 0.7 GPa Young's modulus value obtained for the 20% organic content sample. Based on previous reports for samples with $E \approx 4$ GPa, it is reasonable to assume that these films are capable of withstanding industrial mechanical planarization processes [55].

Since the GISAXS results presented in Fig. 5B demonstrate a comparable structural order and structural dimensions of the mesoporous architectures, it is reasonable to assume that the observed mechanical improvements were not related to altered structural characteristics of the mesoporous films but rather to chelating agent induced improvements in the mechanical properties of the mesoporous films. Indeed, evidence of a denser inorganic network formation, following calcination and removal of the BCP, is observed with the addition of the chelating agent. While water represents a suitable solvent for characterizing sample mesoporosity, its high surface tension makes it less sensitive to changes in the microporosity [85]. To this end, the use of small apolar

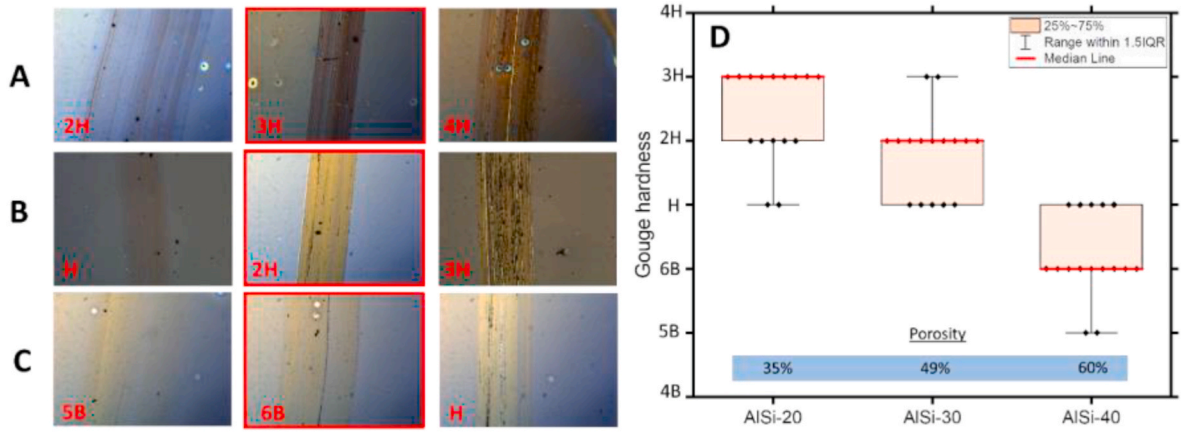

Fig. 3. Pencil scratch tests for aluminosilicate mesoporous samples with different porosity: AlSi-20 (A); AlSi-30 (B) and AlSi-40 (C). Gouge hardness results from repeated batches of samples, where the median value is represented by a red line. (For interpretation of the references to colour in this figure legend, the reader is referred to the Web version of this article.)

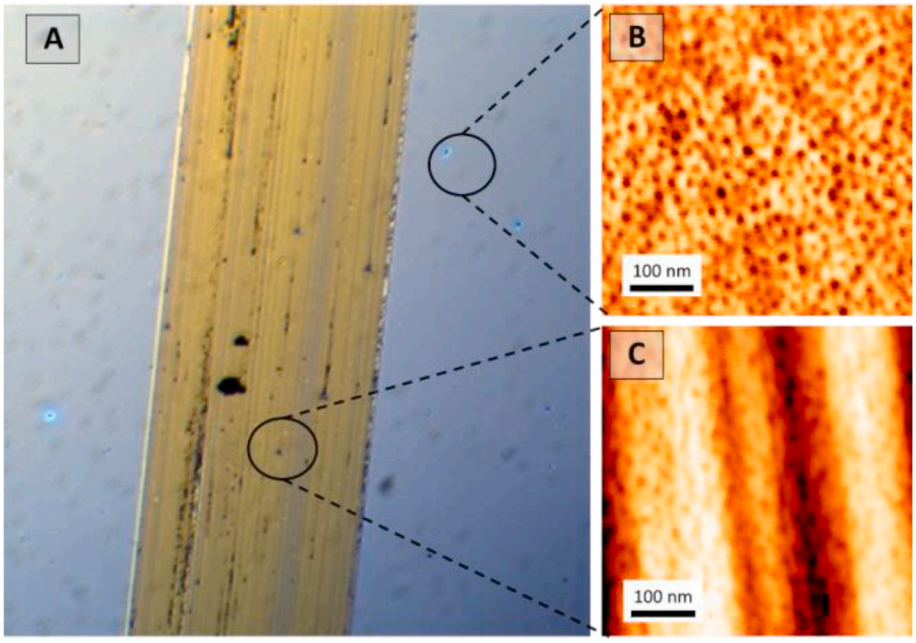

Fig. 4. Optical microscope (A) and AFM images of AlSi-20 aluminosilicate mesoporous films with a chelating agent without scratch (B) and after scratching with 2H pencil (C).

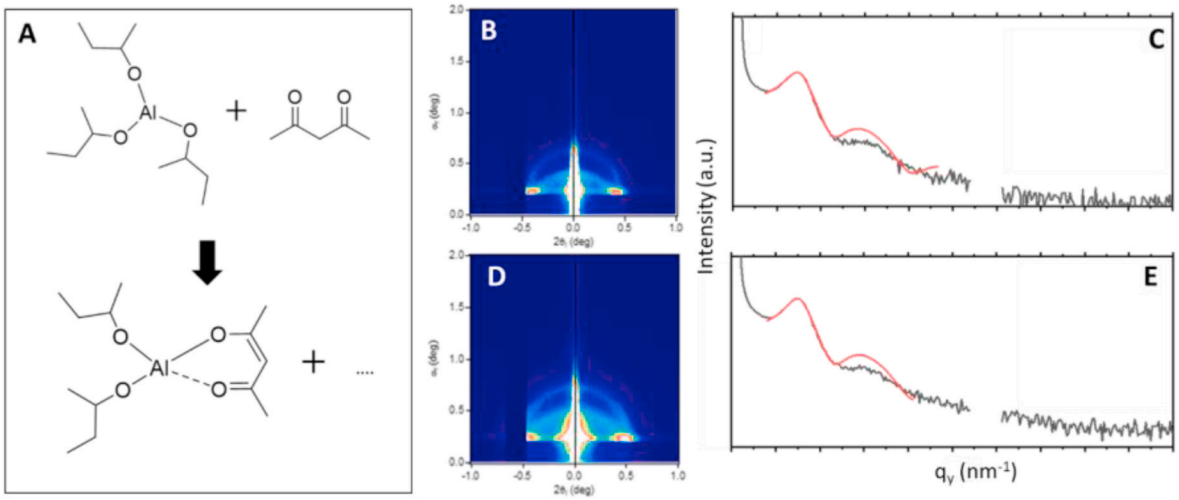

Fig. 5. Schematic representation of the reaction of the aluminium tri-*sec*-butoxide precursor with the acetoacetone chelating agent (A). GISAXS scattering pattern and corresponding 1-dimensional line cut along q_y of a standard aluminosilicate-BCP hybrid film (B–C) and with the presence of the chelating agent (D–E). Radially integrated q(I) plots of GISAXS patterns, which were fitted to a 2D hexagonal paracrystalline array of spherical objects, shown in red. (For interpretation of the references to colour in this figure legend, the reader is referred to the Web version of this article.)

molecules, e.g., methanol, has shown better performance for microporosity detection and characterization [86]. Methanol adsorption isotherms presented in Fig. S7 show a clear decrease in the microporosity with the addition of the chelating agent to the inorganic matrix. This result agrees with the measured refractive index (RI) values shown in Table 1. Although similar mesoporosity values were reported, the RI of the AcAc aluminosilicate mesoporous coatings were higher than the corresponding without the chelating agent. This indicates that a denser inorganic network has formed, following calcination and removal of the BCP.

In order to investigate the effect of densification on the mechanical properties, pencil hardness scratching resistance tests were performed on all coatings. Fig. 7 shows the optical microscopy images of the scratched mesoporous films. In comparison to standard aluminosilicate films shown in the previous section, where gouge hardness rapidly deteriorated from 3H (AlSi-20) to 2H and 6B (AlSi-30 and AlSi-40 respectively); the samples with AcAc showed consistently a higher scratch resistance. Samples of 30% porosity exhibited a gouge hardness of 4H (AcAc-20) (Fig. 7A), decreasing to 3H and 2H for 50 (AcAc-30) and 60% (AcAc-40) porosity respectively (Fig. 7B and C).

In order to confirm the statistical significance of the obtained results, a paired-sample *t*-Test analysis was performed for each pair or values, comparing standard and chelated AlSi respectively at each porosity. In the three cases *p*-values (defined as the probability that the null hypothesis is true, i.e. chelating agents having no effect) close to 0 were obtained: $p_{AlSi\text{-}20\text{-}AcAc\text{-}20} = 5.59 \times 10^{-5}$; $p_{AlSi\text{-}30\text{-}AcAc\text{-}30} = 1.65 \times 10^{-4}$; and $p_{AlSi\text{-}40\text{-}AcAc\text{-}40} = 2.25 \times 10^{-6}$. This allowed us to conclude that the mechanical properties of the samples with chelating agents are different

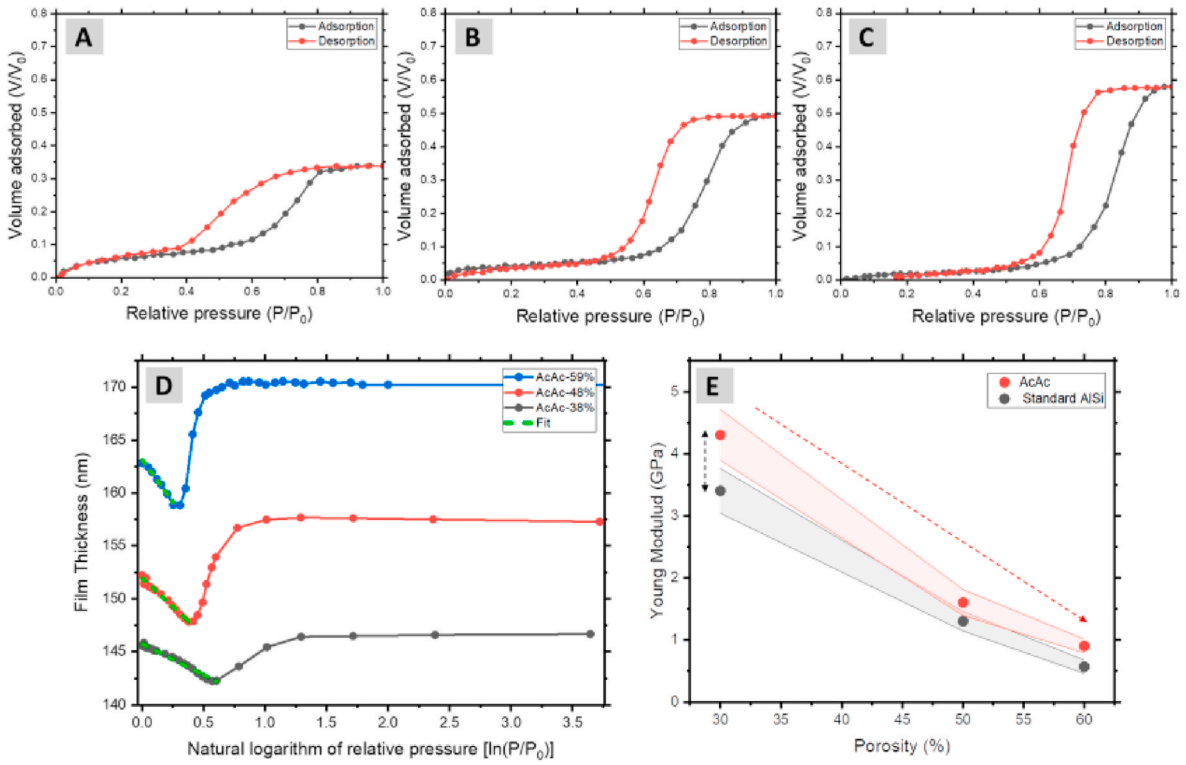

Fig. 6. EP absorption-desorption isotherms (A–C) and corresponding thickness isotherms plotted in the log p/p_0 scale (D) for samples with AcAc chelating agent and different porosity, linear fit shown in green. AcAc-20% (A); AcAc-30% (B) and AcAc-40% (C). Evolution of the Young's modulus with the change in the porosity of the samples (black) and influence of the addition of the chelating agent (red) (E). (For interpretation of the references to colour in this figure legend, the reader is referred to the Web version of this article.)

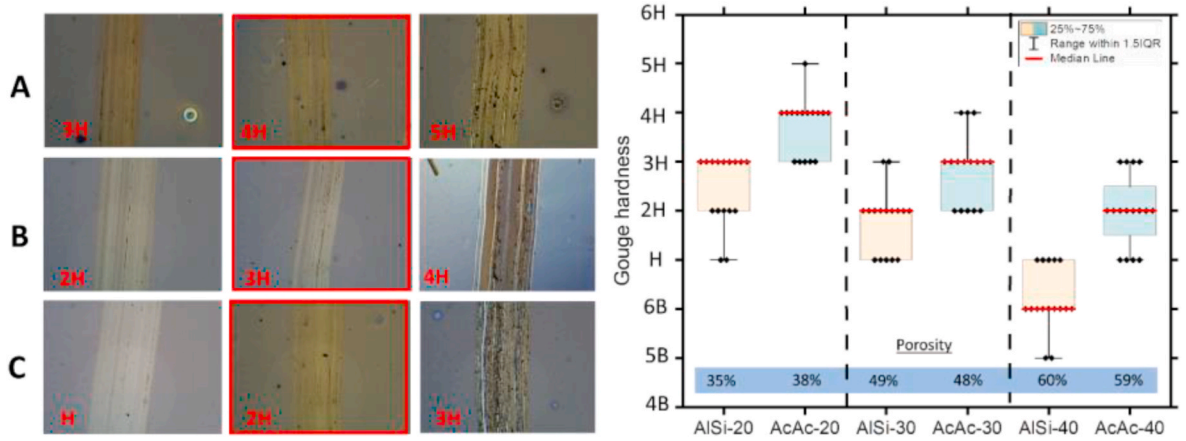

Fig. 7. Pencil scratch tests for aluminosilicate mesoporous samples with AcAc chelating agent and different porosity: AcAc-20 (A); AcAc-30 (B) and AcAc-40 (C). Gouge hardness results from repeated sample batches of previous samples, where the median value is represented by a red line. Previous results with standard AlSi films are presented for direct comparison. (For interpretation of the references to colour in this figure legend, the reader is referred to the Web version of this article.)

from the standard samples, and therefore, the improvements observed in the mechanical properties of the mesoporous films are statistically significant.

We note that there may be additional factors that could be affected by the use of the chelating agent. For the conventional approach, the aluminium is typically found in tetrahedral and octahedral coordination, i.e. evenly distributed in the silicon-framework and in aluminium microdomains, respectively [87]. The ratio may be affected by the chelating agent, which was not in scope of this study. Furthermore, the chelating agent may lead to a greater adhesion of silica surfaces, which could further impact in scratch resistance [39].

3.3. *Effect of two-step calcination*

Recent work has shown the potential of a two-step calcination process, composed of high-temperature treatment in argon followed by air calcination, for enhancing structural order in aluminosilicate mesoporous thin films [88]. The formation of a carbon scaffold during the calcination in argon enables the inorganic matrix to fully condense before template removal during the subsequent oxygen calcination. This independent control over sol-gel condensation reaction and template removal presents a viable route for reducing anisotropic shrinkage due to decreased volume contraction, retaining a higher porosity as well as larger, more uniform pores with extended hexagonally closed-packed

order [88]. This section explores the impact of the aforementioned two-step calcination approach on the thin-film mechanical properties.

In order to establish a direct comparison with previously presented results, similar O:I ratios were used for preparing the hybrid films on silicon substrates. In this case, a two-step calcination process was conducted. The first calcination under argon was followed by another calcination process in ambient atmosphere. The formation of mesoporous films was confirmed by the EP adsorption isotherms shown in Fig. 8. In line with previous observations [88], the two-step calcination led to more porous samples. Thus, for a 20% organic content, porosity increased from the previous 35 ± 0.8 (AlSi-20) to 40 ± 0.9% (Ar-20). The same trend was observed for higher organic content, 59 ± 0.8% (AlSi-30) vs 49 ± 0.6% (Ar-30) for 30% organic content and 68 ± 0.7% (AlSi-40) vs 60 ± 0.5% (Ar-40) for 40% organic content respectively. This is related to the reduction in the anisotropic shrinkage of the film during the calcination process. Importantly, the mean pore sizes remained near constant.

Mechanical properties in terms of Young's modulus and scratching resistance were assessed by EP and pencil scratching test respectively. Similarly to previous sections, the introduction of higher porosity in the films led to a clear deterioration of both Young's modulus (Fig. 8D) and scratching resistance (Fig. 9). However, when these results are compared with those obtained for a one-step calcination, an interesting trend can be observed: at low organic content both *E* and scratching resistance values followed the same trend as for the one-step calcination, but at higher organic content the deterioration of the mechanical properties of the film was slowed down with the introduction of the two-step calcination approach (Fig. 8E).

This is related to the effect of the carbon scaffold formed during the argon calcination step. High organic content meant that more carbon was formed during the first calcination step, and therefore the effect of this factor in the stabilization of the mesoporous structure was more important. Structural stability of high porosity films >60% is generally compromised by the fast removal of the BCP template compared to the time scale of the sol-gel reaction kinetics. The introduction of the two-step calcination step process allowed the independent control over condensation reaction (argon) and template removal (oxygen), leading to an improvement in the structural order of the high porous films and therefore increasing their mechanical stability. The same trend was observed also during pencil scratching tests (Fig. 9). Similar hardness (3H) values were obtained at low organic content (Ar-20), even if two-step calcination samples presented a higher porosity. However, when organic content increased, a clear improvement in the mechanical stability of the mesoporous films was observed. Interestingly, with a 40% organic content, and porosity values of 68% (close to an ideal hexagonal close-packed structure of 74%), the carbon scaffolding presented during the Ar calcination allowed for an improvement of the Gouge hardness of the films from 6B (AlSi-40) to H (Ar-40) despite a ≈10% higher porosity compared to the one-step counterpart.

3.4. *Overview - improving mechanical properties of aluminosilicate thin films*

Table 2 shows all the structural and mechanical characteristics of the samples studied during this work. The results corroborate other reported studies regarding the detrimental impact of increased porosity on scratch and mechanical characteristics of the material. However, the BCP co-assembly strategy allows for a complete control over the structural characteristics of the obtained mesoporous thin films (porosity, pore arrangement, size of pores and interconnections, wall thickness), promoting the generation of highly tuneable mesoporous architectures. The incorporation of the chelating agent acetylacetone allowed control over the kinetics of the sol-gel hydrolysis, leading to an improvement in the mechanical characteristics of the mesoporous thin films, related to

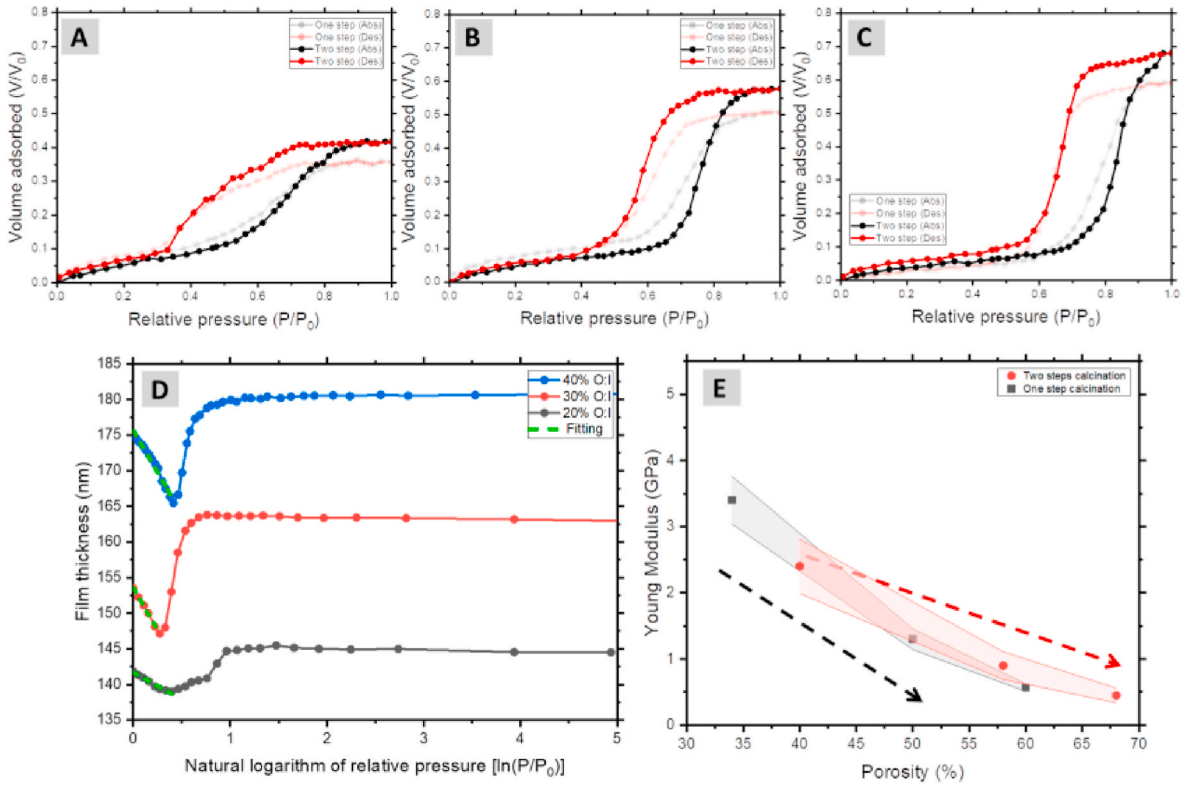

Fig. 8. EP absorption-desorption isotherms (A–C) and corresponding thickness isotherms plotted in the log p/p_0 scale (D) for samples with different porosity after the two-step calcination, linear fit shown in green: Ar-20 (A); Ar-30 (B) and Ar-40 (C). Absorption-desorption isotherms of the standard one-step calcination process are presented for direct comparison. The evolution of the Young's modulus is plotted in (E) following a one-step (black) and a two-step (red) calcination approach. (For interpretation of the references to colour in this figure legend, the reader is referred to the Web version of this article.)

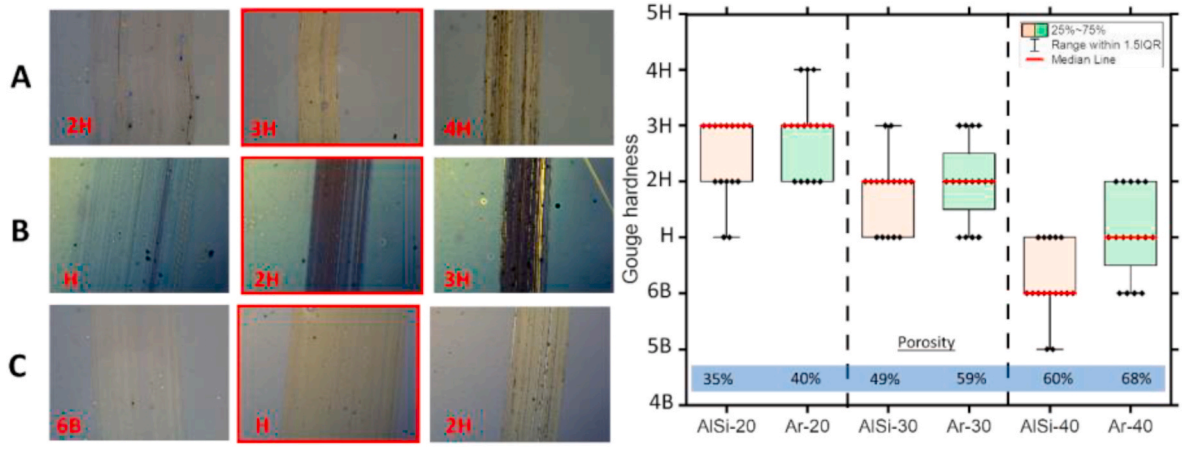

Fig. 9. Pencil scratch tests for aluminosilicate mesoporous samples with different porosity after the two-step calcination: Ar-20 (A); Ar-30 (B) and Ar-40 (C). Gouge hardness results from repeated sample batches, where the median value is represented by a red line. Previous results with standard calcination process are presented for comparison. It is important to note that contrary to previous investigations, here the porosity values are different. (For interpretation of the references to colour in this figure legend, the reader is referred to the Web version of this article.)

Table 2
Summary of all the structural and mechanical parameters studied during this work: Organic content, porosity, refractive index (at 632.8 nm^{-1}), pore size, thickness, Young's modulus, and gouge hardness.

	Organic content (%)	Porosity (%)	RI	PS (nm)	T (nm)	E (GPa)	Hardness
Porosity variation	20	35 ± 0.8	1.23	7.2 ± 0.1	123 ± 0.4	3.4 ± 0.5	3H
	30	49 ± 0.6	1.17	8.2 ± 0.3	120 ± 0.8	1.3 ± 0.1	2H
	40	60 ± 0.5	1.13	10 ± 0.1	97 ± 0.4	0.6 ± 0.1	6 B
Addition of chelating agent	20	38 ± 0.7	1.28	7.8 ± 0.2	93 ± 1.3	4.3 ± 0.7	4H
	30	48 ± 0.6	1.20	8.6 ± 0.3	87 ± 0.5	1.6 ± 0.2	3H
	40	59 ± 0.8	1.17	10.9 ± 0.5	77 ± 0.3	0.9 ± 0.1	2H
Two-step calcination	20	40 ± 0.9	1.24	9.5 ± 0.8	150 ± 1.2	2.4 ± 0.3	3H
	30	59 ± 0.5	1.20	9.7 ± 0.3	147 ± 2.5	0.9 ± 0.2	2H
	40	68 ± 0.7	1.16	12.0 ± 0.2	132 ± 1.5	0.4 ± 0.2	H

the creation of denser aluminosilicate networks. The modification of the fabrication conditions by the addition of a two-step calcination procedure enabled the creation of aluminosilicate thin films with porosities close to 70% and with improved mechanical properties.

4. Conclusions

Improving the scratch resistance and mechanical characteristics of mesoporous thin films remains a fundamental challenge to long-term coating performance. This work described the influence of material porosity, chemistry, and processing conditions on the mechanical characteristics of the final porous material. Evaluation was performed by qualitative pencil scratch tests and quantitative determination of the Young's modulus via EP, which represents a non-destructive and high-sensitive platform for structural and mechanical thin film characterization. Interestingly, the addition of organic chelating agents to the aluminosilicate sol-gel recipe slowed the hydrolysis of the aluminium precursor, leading to a densification of the inorganic network, i.e. loss in microporosity while retaining its mesoporous characteristics. As a result, these coatings exhibit mechanical properties close to industrial standards. Moreover, a two-step calcination process with initial high-temperature treatment in an inert atmosphere provides an additional mean to improve the structural integrity, in particular of highly porous samples, i.e. in the range of 60%–70%. These results demonstrate the versatility of BCP/sol-gel co-assembly, not only as a highly tuneable fabrication route for mesoporous thin films but also by providing amenable processing steps for enhanced mechanical properties. With aluminosilicate mesoporous thin films being used in demanding applications such as bio-/chemosensors or optical coatings, insights presented herein about their enhanced mechanical properties will enable improvements in their long-term performance.

CRediT authorship contribution statement

Barry Reid: Writing – original draft, Methodology, Investigation, Formal analysis, Data curation, Conceptualization. **Ishaa Mane:** Investigation, Formal analysis, Data curation. **Faizah Ahmed:** Investigation, Formal analysis, Data curation. **Maximiliano Jara Fornerod:** Writing – review & editing, Methodology, Investigation, Formal analysis, Data curation. **Máté Füredi:** Investigation, Formal analysis, Data curation. **Benjamin Schmidt-Hansberg:** Conceptualization, Methodology, Supervision, Writing – review & editing. **Alberto Alvarez-Fernandez:** Writing – original draft, Supervision, Project administration, Investigation, Conceptualization. **Stefan Guldin:** Writing – review & editing, Supervision, Resources, Project administration, Methodology, Funding acquisition, Conceptualization.

Declaration of competing interest

The authors declare the following financial interests/personal relationships which may be considered as potential competing interests: Guldin reports financial support was provided by Engineering and Physical Sciences Research Council. Guldin reports financial support was provided by BASF SE.

Data availability

Data will be made available on request.

Acknowledgments

A.A.F., M.J.F., and S.G. acknowledge funding by the EPSRC New Investigator Award (EP/R035105/1). B.R. was supported by an EPSRC Industrial Case Award (EP/M506448/1) in support of BASF. M.J.F acknowledge the support of the Henry Royce Institute through the Royce PhD Equipment Access Scheme enabling access to microscopy facilities at Royce@Cambridge; EPSRC Grant Number EP/R00661X/1.

Appendix A. Supplementary data

Supplementary data to this article can be found online at https://doi.org/10.1016/j.micromeso.2022.112246.

References

[1] W. Li, J. Liu, D. Zhao, Mesoporous materials for energy conversion and storage devices, Nat. Rev. Mater. 1 (2016), 16023, https://doi.org/10.1038/natrevmats.2016.23.
[2] S. Guldin, P. Kohn, M. Stefik, J. Song, G. Divitini, F. Ecarla, C. Ducati, U. Wiesner, U. Steiner, Self-cleaning antireflective optical coatings, Nano Lett. 13 (2013) 5329–5335, https://doi.org/10.1021/nl402832u.
[3] B. Reid, A. Taylor, Y. Chen, B. Schmidt-Hansberg, S. Guldin, Robust operation of mesoporous antireflective coatings under variable ambient conditions, ACS Appl. Mater. Interfaces 10 (2018) 10315–10321, https://doi.org/10.1021/acsami.7b18299.
[4] D. Karthik, S. Pendse, S. Sakthivel, E. Ramasamy, S.V. Joshi, High performance broad band antireflective coatings using a facile synthesis of ink-bottle mesoporous MgF2 nanoparticles for solar applications, Sol. Energy Mater. Sol. Cells 159 (2017) 204–211, https://doi.org/10.1016/J.SOLMAT.2016.08.007.
[5] S. Guldin, M. Kolle, M. Stefik, R. Langford, D. Eder, U. Wiesner, U. Steiner, Tunable mesoporous bragg reflectors based on block-copolymer self-assembly, Adv. Mater. 23 (2011) 3664–3668, https://doi.org/10.1002/adma.201100640.
[6] G. Kaune, M. Haese-Seiller, R. Kampmann, J.F. Moulin, Q. Zhong, P. Müller-Buschbaum, Tof-gisans investigation of polymer infiltration in mesoporous TiO 2 films for photovoltaic applications, J. Polym. Sci. B Polym. Phys. 48 (2010) 1628–1635, https://doi.org/10.1002/polb.21964.
[7] X. Yang, P. Qiu, J. Yang, Y. Fan, L. Wang, W. Jiang, X. Cheng, Y. Deng, W. Luo, Mesoporous materials–based electrochemical biosensors from enzymatic to nonenzymatic, Small 17 (2021), 1904022, https://doi.org/10.1002/smll.201904022.
[8] G. Zhou, K.K. Fung, L.W. Wong, Y. Chen, R. Renneberg, S. Yang, Immobilization of glucose oxidase on rod-like and vesicle-like mesoporous silica for enhancing current responses of glucose biosensors, Talanta 84 (2011) 659–665, https://doi.org/10.1016/j.talanta.2011.01.058.
[9] K.S. Jang, H.J. Kim, J.R. Johnson, W.G. Kim, W.J. Koros, C.W. Jones, S. Nair, Modified mesoporous silica gas separation membranes on polymeric hollow fibers, Chem. Mater. 23 (2011) 3025–3028, https://doi.org/10.1021/cm200939d.
[10] D. Lee, M.F. Rubner, R.E. Cohen, All-nanoparticle thin-film coatings, Nano Lett. 6 (2006) 2305–2312, https://doi.org/10.1021/NL061776M/SUPPL_FILE/NL061776MSI20060825_103338.PDF.
[11] S. Colodrero, M. Ocaña, H. Míguez, Nanoparticle-based one-dimensional photonic crystals, Langmuir 24 (2008) 4430–4434, https://doi.org/10.1021/LA703987R/SUPPL_FILE/LA703987R-FILE003.PDF.
[12] L. Huang, M. Kruk, Versatile surfactant/swelling-agent template for synthesis of large-pore ordered mesoporous silicas and related hollow nanoparticles, Chem. Mater. 27 (2015) 679–689, https://doi.org/10.1021/cm5028749.
[13] X. Meng, Y. Wang, H. Wang, J. Zhong, R. Chen, Preparation of hydrophobic and abrasion-resistant silica antireflective coatings by using a cationic surfactant to regulate surface morphologies, Sol. Energy 101 (2014) 283–290, https://doi.org/10.1016/J.SOLENER.2013.12.038.
[14] K.W. Park, J.Y. Kim, H.J. Seo, O.Y. Kwon, Preparation of mesoporous silica by nonionic surfactant micelle–templated gelation of Na2SiO3 and H2SiF6 and application as a catalyst carrier for the partial oxidation of CH4, Sci. Rep. 9 (2019) 1–8, https://doi.org/10.1038/s41598-019-50053-y.
[15] S. Leyva-García, D. Lozano-Castelló, E. Morallón, D. Cazorla-Amorós, Silica-templated ordered mesoporous carbon thin films as electrodes for micro-capacitors, J Mater Chem A Mater 4 (2016) 4570–4579, https://doi.org/10.1039/C5TA10552H.
[16] P. Innocenzi, S. Costacurta, T. Kidchob, L. Malfatti, P. Falcaro, G. Soler-Illia, Mesoporous thin films: properties and applications, in: Thin Films, Springer, Dordrecht, 2008, pp. 105–123, https://doi.org/10.1007/978-1-4020-8514-7_7.
[17] B. Hatton, L. Mishchenko, S. Davis, K.H. Sandhage, J. Aizenberg, Assembly of large-area, highly ordered, crack-free inverse opal films, Proc. Natl. Acad. Sci. U. S. A. 107 (2010) 10354–10359, https://doi.org/10.1073/pnas.1000954107.
[18] P.C. Alberius, K.L. Frindell, R.C. Hayward, E.J. Kramer, G.D. Stucky, B.F. Chmelka, General predictive syntheses of cubic, hexagonal, and lamellar silica and titania mesostructured thin films, Chem. Mater. 14 (2002) 3284–3294, https://doi.org/10.1021/cm011209u.
[19] E.L. Crepaldi, G.J.A.A Soler-Illia, D. Grosso, F. Cagnol, F. Ribot, C. Sanchez, Controlled formation of highly organized mesoporous titania thin films: from mesostructured hybrids to mesoporous nanoanatase TiO 2, J. Am. Chem. Soc. 125 (2003) 9770–9786, https://doi.org/10.1021/ja030070g.
[20] D.F. Lionello, J.I. Ramallo, G.J.A.A. Soler-Illia, M.C. Fuertes, Mechanical properties of ordered mesoporous oxides thin films, J. Sol. Gel Sci. Technol. 101 (2021) 114–139, https://doi.org/10.1007/S10971-021-05626-7, 1. 101 (2021).
[21] C.-T. Tsai, H.-Y. Lu, C.-Y. Ting, W.-F. Wu, B.-Z. Wan, Increasing mechanical strength of mesoporous silica thin films by addition of tetrapropylammonium hydroxide and refluxing processes, Thin Solid Films 517 (2009) 2039–2043, https://doi.org/10.1016/j.tsf.2008.10.012.
[22] U. Schubert, N. Huesing, A. Lorenz, Hybrid inorganic-organic materials by sol-gel processing of organofunctional metal alkoxides, Chem. Mater. 7 (1995) 2010, https://doi.org/10.1021/cm00059a007. –2027.
[23] K. Wang, J. He, One-pot fabrication of antireflective/antibacterial dual-function Ag NP-containing mesoporous silica thin films, ACS Appl. Mater. Interfaces 10 (2018) 11189–11196, https://doi.org/10.1021/acsami.8b00192.
[24] L.Y.L. Wu, E. Chwa, Z. Chen, X.T. Zeng, A study towards improving mechanical properties of sol–gel coatings for polycarbonate, Thin Solid Films 516 (2008) 1056–1062, https://doi.org/10.1016/j.tsf.2007.06.149.
[25] K.C. Song, J.K. Park, H.U. Kang, S.H. Kim, Synthesis of hydrophilic coating solution for polymer substrate using glycidoxypropyltrimethoxysilane, J. Sol. Gel Sci. Technol. 27 (2003) 53–59, https://doi.org/10.1023/A:1022679910313.
[26] Y. Xu, C. Peng, C. Xin, J. Wu, Preparation of silica antireflective films for solar energy application, Mater. Lett. 94 (2013) 89–91, https://doi.org/10.1016/j.matlet.2012.12.013.
[27] G.J.A.A. Soler-Illia, O. Azzaroni, Multifunctional hybrids by combining ordered mesoporous materials and macromolecular building blocks, Chem. Soc. Rev. 40 (2011) 1107, https://doi.org/10.1039/c0cs00208a.
[28] N. Chemin, M. Klotz, V. Rouessac, A. Ayral, E. Barthel, Mechanical properties of mesoporous silica thin films: effect of the surfactant removal processes, Thin Solid Films 495 (2006) 210–213, https://doi.org/10.1016/j.tsf.2005.08.260.
[29] K. Vanstreels, C. Wu, M.R. Baklanov, Mechanical stability of porous low-k dielectrics, ECS J. Solid State Sci. Technol. 4 (2015) N3058–N3064, https://doi.org/10.1149/2.0071501jss.
[30] X. Li, J.C. Birnbaum, R.E. Williford, G.E. Fryxell, C.A. Coyle, G.C. Dunham, S. Baskaran, Effect of humidity treatments on porosity and mechanical integrity of mesoporous silica films, Chem 3 (2003) 2054, https://doi.org/10.1039/b304843h.
[31] J. Sun, Q. Zhang, R. Ding, H. Lv, H. Yan, X. Yuan, Y. Xu, Contamination-resistant silica antireflective coating with closed ordered mesopores, Phys. Chem. Chem. Phys. 16 (2014) 16684–16693, https://doi.org/10.1039/C4CP01032A.
[32] M. Boudot, V. Gaud, M. Louarn, M. Selmane, D. Grosso, Sol–gel based hydrophobic antireflective coatings on organic substrates: a detailed investigation of ammonia vapor treatment (avt), Chem. Mater. 26 (2014) 1822–1833, https://doi.org/10.1021/cm403787v.
[33] T.-J. Ha, H.-H. Park, S.-B. Jung, H. Ryu, B.-G. Yu, Investigation of the effect of calcination temperature on HMDS-treated ordered mesoporous silica film, J. Colloid Interface Sci. 326 (2008) 186–190, https://doi.org/10.1016/j.jcis.2008.07.024.
[34] N. Nishiyama, S. Tanaka, Y. Egashira, Y. Oku, K. Ueyama, Enhancement of structural stability of mesoporous silica thin films prepared by spin-coating, Chem. Mater. 14 (2002) 4229–4234, https://doi.org/10.1021/cm0201246.
[35] J.Y. Chen, F.M. Pan, A.T. Cho, K.J. Chao, T.G. Tsai, B.W. Wu, C.M. Yang, L. Chang, Microstructure and mechanical properties of surfactant templated nanoporous silica thin films: effect of methylsilylation, J. Electrochem. Soc. 150 (2003) F123, https://doi.org/10.1149/1.1573200/XML.
[36] M. Righeira Carnegie, A. Sherine, D. Sivagami, S. Sakthivel, Anti-reflection coatings with enhanced abrasion and scratch resistance properties, J. Sol. Gel Sci. Technol. 78 (2016) 176–186, https://doi.org/10.1007/S10971-015-3924-9/TABLES/4.
[37] L. Xu, Z. Geng, J. He, G. Zhou, Mechanically robust, thermally stable, broadband Antireflective, and superhydrophobic thin films on glass substrates, ACS Appl. Mater. Interfaces 6 (2014) 9029, https://doi.org/10.1021/am5016777. –9035.
[38] L. Miao, L.F. Su, S. Tanemura, C.A.J. Fisher, L.L. Zhao, Q. Liang, G. Xu, Cost-effective nanoporous SiO2–TiO2 coatings on glass substrates with antireflective and self-cleaning properties, Appl. Energy 112 (2013) 1198–1205, https://doi.org/10.1016/j.apenergy.2013.03.043.
[39] R. Nass, H. Schmidt, Synthesis of an alumina coating from chelated aluminium alkoxides, J. Non-Cryst. Solids 121 (1990) 329–333, https://doi.org/10.1016/0022-3093(90)90153-D.
[40] L. Bonhomme-Coury, F. Babonneau, J. Livage, Investigation of the sol-gel chemistry of ethylacetoacetate modified aluminum sec-butoxide, J. Sol. Gel Sci. Technol. 3 (1994) 157–168, https://doi.org/10.1007/BF00486555, 3. 3 (1994).
[41] J. Livage, C. Sanchez, Sol-gel chemistry, J. Non-Cryst. Solids 145 (1992) 11–19, https://doi.org/10.1016/S0022-3093(05)80422-3.
[42] L. Ji, J. Lin, K.L. Tan, H.C. Zeng, Synthesis of high-surface-area alumina using aluminum tri-sec-butoxide-2,4-pentanedione-2-propanol-nitric acid precursors, Chem. Mater. 12 (2000) 931–939, https://doi.org/10.1021/CM990404U/ASSET/IMAGES/LARGE/CM990404UF00009 (JPEG).
[43] A. Mitra, D. Jana, G. De, A facile synthesis of cubic (Imm) alumina films on glass with potential catalytic activity, Chem. Commun. (J. Chem. Soc. Sect. D) 48 (2012) 3333–3335, https://doi.org/10.1039/C2CC18053G.
[44] B. Zhang, Q. Guo, B. Dai, N. Wang, Y. Dai, Y. Qi, Dependence of the structure of Bi-2212 superconducting thin film prepared by sol-gel method on different complexing agents, Ceram. Int. (2022), https://doi.org/10.1016/J.CERAMINT.2022.05.025.
[45] J. Moghal, J. Kobler, J. Sauer, J. Best, M. Gardener, A.A.R. Watt, G. Wakefield, High-performance, single-layer antireflective optical coatings comprising

mesoporous silica nanoparticles, ACS Appl. Mater. Interfaces 4 (2012) 854–859, https://doi.org/10.1021/am201494m.
[46] J. Wang, G.G. Wu, J. Shen, T. Yang, Q. Zhang, B. Zhou, Z. Deng, B. Fan, D. Zhou, F. Zhang, Scratch-Resistant improvement of sol-gel derived nano-porous silica films, J. Sol. Gel Sci. Technol. 18 (2000) 219–224, https://doi.org/10.1023/A:1008787722437, 3. 18 (2000).
[47] L. Yao, J. He, Z. Geng, T. Ren, Fabrication of mechanically robust, self-cleaning and optically high-performance hybrid thin films by SiO2&TiO2 double-shelled hollow nanospheres, Nanoscale 7 (2015) 13125–13134, https://doi.org/10.1039/C5NR02467F.
[48] A. Ershad-langroudi, C. Mai, G. Vigier, R. Vassoille, Laboratoire GEMPPM umr, hydrophobic hybrid inorganic-organic thin film prepared by sol-gel process for glass protection and strengthening applications, J. Appl. Polym. Sci. 65 (1997) 2387–2393, https://doi.org/10.1002/(SICI)1097-4628 (19970919)65:12.
[49] K.H. Nielsen, S. Karlsson, R. Limbach, L. Wondraczek, Quantitative image analysis for evaluating the abrasion resistance of nanoporous silica films on glass, Sci. Rep. 5 (2015), 17708, https://doi.org/10.1038/srep17708.
[50] R.L. Browning, G.-T. Lim, A. Moyse, H.-J. Sue, H. Chen, J.D. Earls, Quantitative evaluation of scratch resistance of polymeric coatings based on a standardized progressive load scratch test, Surf. Coat. Technol. 201 (2006) 2970–2976, https://doi.org/10.1016/j.surfcoat.2006.06.007.
[51] W. Volksen, K. Lionti, T. Magbitang, G. Dubois, Hybrid low dielectric constant thin films for microelectronics, Scripta Mater. 74 (2014) 19–24, https://doi.org/10.1016/J.SCRIPTAMAT.2013.05.025.
[52] M. Darnon, N. Casiez, T. Chevolleau, G. Dubois, W. Volksen, T.J. Frot, R. Hurand, T.L. David, N. Posseme, N. Rochat, C. Licitra, Impact of low-k structure and porosity on etch processes, J. Vac. Sci. Technol., B: Nanotechnol. Microelectron. 31 (2013), 011207, https://doi.org/10.1116/1.4770505.
[53] M.R. Baklanov, C. Adelmann, L. Zhao, S. de Gendt, Advanced interconnects: materials, processing, and reliability, ECS J. Sol. State Sci. Technol. 4 (2015) Y1–Y4, https://doi.org/10.1149/2.0271501JSS/XML.
[54] D. Shamiryan, T. Abell, F. Iacopi, K. Maex, Low-k dielectric materials, Mater. Today 7 (2004) 34–39, https://doi.org/10.1016/S1369-7021(04)00053-7.
[55] G. Dubois, W. Volksen, T. Magbitang, R.D. Miller, D.M. Gage, R.H. Dauskardt, Molecular network reinforcement of sol–gel glasses, Adv. Mater. 19 (2007) 3989–3994, https://doi.org/10.1002/ADMA.200701193.
[56] R. Saha, W.D. Nix, Effects of the substrate on the determination of thin film mechanical properties by nanoindentation, Acta Mater. 50 (2002) 23–38, https://doi.org/10.1016/S1359-6454(01)00328-7.
[57] C. Sanchez, C. Boissière, D. Grosso, C. Laberty, L. Nicole, Design, synthesis, and properties of inorganic and hybrid thin films having periodically organized nanoporosity, Chem. Mater. 20 (2008) 682–737, https://doi.org/10.1021/CM702100T/ASSET/IMAGES/LARGE/CM-2007-02100T_0029 (JPEG).
[58] K. Lionti, K. Virwani, W. Volksen, R. King, J. Frommer, G. Dubois, Accurate measurement of porous low-k thin-films by nanoindentation: densification scaling versus substrate effects, ECS J. Sol. State Sci. Technol. 6 (2017) N209–N212, https://doi.org/10.1149/2.0151710JSS/XML.
[59] J.I. Ramallo, J. Morrone, D.F. Lionello, P.C. Angelomé, M.C. Fuertes, Mechanical properties and structural integrity of devices based on sol–gel mesoporous oxides thin films, J. Sol. Gel Sci. Technol. 102 (2021) 185–196, https://doi.org/10.1007/S10971-021-05636-5/FIGURES/5.
[60] A.M. Urbanowicz, B. Meshman, D. Schneider, M.R. Baklanov, Stiffening and hydrophilisation of SOG low-k material studied by ellipsometric porosimetry, UV ellipsometry and laser-induced surface acoustic waves, Phys. Status Solidi 205 (2008) 829–832, https://doi.org/10.1002/PSSA.200777749.
[61] C. Murray, C. Flannery, I. Streiter, S.E. Schulz, M.R. Baklanov, K.P. Mogilnikov, C. Himcinschi, M. Friedrich, D.R.T. Zahn, T. Gessner, Comparison of techniques to characterise the density, porosity and elastic modulus of porous low-k SiO2 xerogel films, Microelectron. Eng. 60 (2002) 133–141, https://doi.org/10.1016/S0167-9317(01)00589-5.
[62] C.M. Flannery, T. Wittkowski, K. Jung, B. Hillebrands, M.R. Baklanov, Critical properties of nanoporous low dielectric constant films revealed by Brillouin light scattering and surface acoustic wave spectroscopy, Appl. Phys. Lett. 80 (2002) 4594–4596, https://doi.org/10.1063/1.1478775.
[63] K. Uchino, The development of piezoelectric materials and the new perspective, Advanced Piezoelectric Materials, Sci. Technol. (2010) 1–85, https://doi.org/10.1533/9781845699758.1.
[64] K. Maex, M.R. Baklanov, D. Shamiryan, F. Iacopi, S.H. Brongersma, Z. S. Yanovitskaya, Low dielectric constant materials for microelectronics, J. Appl. Phys. 93 (2003) 8793, https://doi.org/10.1063/1.1567460.
[65] C. Boissiere, D. Grosso, S. Lepoutre, L. Nicole, A. Brunet Bruneau, C. Sanchez, Porosity and mechanical properties of mesoporous thin films assessed by environmental ellipsometric porosimetry, Langmuir 21 (26) (2005) 12362–12371, https://doi.org/10.1021/la050981z.
[66] M.R. Baklanov, D. Shamiryan, Nondestructive Evaluation of Critical Properties of Thin Porous Films. Porous Polymers, John Wiley & Sons, Inc., 2011, pp. 205–245.
[67] A. Alvarez-Fernandez, B. Reid, J. Suthar, S.Y. Choy, M. Jara Fornerod, N. mac Fhionnlaoich, L. Yang, B. Schmidt-Hansberg, S. Guldin, Fractionation of block copolymers for pore size control and reduced dispersity in mesoporous inorganic thin films, Nanoscale 12 (2020) 18455–18462, https://doi.org/10.1039/d0nr05132b.
[68] M. Templin, A. Franck, A. du Chesne, H. Leist, Y. Zhang, R. Ulrich, V. Schädler, U. Wiesner, Organically modified aluminosilicate mesostructures from block copolymer phases, Science (1979) 1795–1798, https://doi.org/10.1126/SCIENCE.278.5344.1795/ASSET/83683333-B862-4720-A500-5B9519EE6468/ASSETS/GRAPHIC/SE4976057004, 278 (1997 (JPEG).
[69] H.N. Lokupitiya, A. Jones, B. Reid, S. Guldin, M. Stefik, Ordered mesoporous to macroporous oxides with tunable isomorphic architectures: solution criteria for persistent micelle templates, Chem. Mater. 28 (2016) 1653–1667, https://doi.org/10.1021/acs.chemmater.5b04407.
[70] T. von Graberg, P. Hartmann, A. Rein, S. Gross, B. Seelandt, C. Röger, R. Zieba, A. Traut, M. Wark, J. Janek, B. Smarsly, Mesoporous tin-doped indium oxide thin films: effect of mesostructure on electrical conductivity, Sci. Technol. Adv. Mater. 12 (2) (2011) 025005, https://doi.org/10.1088/1468-6996/12/2/025005.
[71] A. Alvarez-Fernandez, M.J. Fornerod, B. Reid, S. Guldin, Solvent vapor annealing for controlled pore expansion of block copolymer-assembled inorganic mesoporous films, Langmuir 38 (2022) 3297–3304, https://doi.org/10.1021/acs.langmuir.2c00074.
[72] B. Reid, A. Alvarez-Fernandez, B. Schmidt-Hansberg, S. Guldin, Tuning pore dimensions of mesoporous inorganic films by homopolymer swelling, Langmuir 35 (2019) 14074–14082, https://doi.org/10.1021/acs.langmuir.9b03059.
[73] A. Alvarez-Fernandez, B. Reid, M.J. Fornerod, A. Taylor, G. Divitini, S. Guldin, Structural characterization of mesoporous thin film architectures: a tutorial overview, ACS Appl. Mater. Interfaces 12 (2020) 5195–5208, https://doi.org/10.1021/acsami.9b17899.
[74] B. Reid, A. Taylor, A. Alvarez-Fernandez, M.H. Ismael, S. Sharma, B. Schmidt-Hansberg, S. Guldin, Photocatalytic template removal by non-ozone-generating UV irradiation for the fabrication of well-defined mesoporous inorganic coatings, ACS Appl. Mater. Interfaces 11 (2019) 19308–19314, https://doi.org/10.1021/acsami.9b01199.
[75] ASTM International, Standard Test Method for Film Hardness by Pencil Test 1, 2010, pp. 5–7. ASTM D3363-05 Stand. 05.
[76] J. Dendooven, K. Devloo-Casier, E. Levrau, R. Van Hove, S. Pulinthanathu Sree, M. R. Baklanov, J.A. Martens, C. Detavernier, *In Situ* monitoring of atomic layer deposition in nanoporous thin films using ellipsometric porosimetry, Langmuir 28 (8) (2012) 3852–3859, https://doi.org/10.1021/la300045z.
[77] K.P. Mogilnikov, M.R. Baklanov, Determination of Young's modulus of porous low-k films by ellipsometric porosimetry, Electrochem. Solid State Lett. 5 (2002) F29, https://doi.org/10.1149/1.1517771/XML.
[78] D. Babonneau, FitGISAXS: software package for modelling and analysis of GISAXS data using IGOR Pro, J. Appl. Crystallogr. 43 (2010) 929–936, https://doi.org/10.1107/S0021889810020352.
[79] T. Galy, M. Marszewski, S. King, Y. Yan, S.H. Tolbert, L. Pilon, Comparing methods for measuring thickness, refractive index, and porosity of mesoporous thin films, Microporous Mesoporous Mater. 291 (2020), 109677, https://doi.org/10.1016/j.micromeso.2019.109677.
[80] A. Augurio, A. Alvarez-Fernandez, V. Panchal, B. Pittenger, P. de Wolf, S. Guldin, J. Briscoe, Controlled porosity in ferroelectric $BaTiO_3$ photoanodes, ACS Appl. Mater. Interfaces (2022), https://doi.org/10.1021/acsami.1c17419 acsami.1c17419.
[81] M.R. Baklanov, K.P. Mogilnikov, V.G. Polovinkin, F.N. Dultsev, Determination of pore size distribution in thin films by ellipsometric porosimetry, J. Vac. Sci. Technol., B: Microelectronics and Nanometer Structures 18 (2000) 1385–1391, https://doi.org/10.1116/1.591390.
[82] K. Vanstreels, C. Wu, P. Verdonck, M.R. Baklanov, Intrinsic effect of porosity on mechanical and fracture properties of nanoporous ultralow-k dielectrics, Appl. Phys. Lett. 101 (2012), 123109, https://doi.org/10.1063/1.4753972.
[83] S.-B. Jung, H.-H. Park, Concentration-dependent mesostructure of surfactant-templated mesoporous silica thin film, Thin Solid Films 494 (2006) 320–324, https://doi.org/10.1016/j.tsf.2005.08.160.
[84] F. Babonneau, L. Coury, J. Livage, Aluminum sec-butoxide modified with ethylacetoacetate: an attractive precursor for the sol-gel synthesis of ceramics, J. Non-Cryst. Solids 121 (1990) 153–157, https://doi.org/10.1016/0022-3093(90)90122-3.
[85] S. Eslava, M.R. Baklanov, C.E.A. Kirschhock, F. Iacopi, S. Aldea, K. Maex, J. A. Martens, Characterization of a molecular sieve coating using ellipsometric porosimetry, Langmuir 23 (2007) 12811–12816, https://doi.org/10.1021/LA7028388/ASSET/IMAGES/LARGE/LA7028388F00006. JPEG.
[86] M.R. Baklanov, K.P. Mogilnikov, Characterisation of low-K dielectric films by ellipsometric porosimetry, MRS Online Proc. Libr. 612 (2000) 421–4212, https://doi.org/10.1557/PROC-612-D4.2.1, 1. 612 (2000).
[87] S.M. de Paul, J.W. Zwanziger, R. Ulrich, U. Wiesner, H.W. Spiess, Structure, mobility, and interface characterization of self-organized organic-inorganic hybrid materials by solid-state NMR, J. Am. Chem. Soc. 121 (1999) 5727–5736, https://doi.org/10.1021/JA984389Q/ASSET/IMAGES/MEDIUM/JA984389QE00004.GIF.
[88] M.J. Fornerod, A. Alvarez-Fernandez, M.W.A. Skoda, B. Prieto-Simon, N. H. Voelcker, M.-O. Coppens, S. Guldin, Enhanced structural control of soft-templated mesoporous inorganic thin films by inert processing conditions. https://doi.org/10.26434/CHEMRXIV-2022-C0PLP, 2022.